Article ID: 1000-324X(2017)01-0107-06 **DOI:** 10.15541/jim20160143

Sol-Gel-derived Mesoporous Calcium Aluminum Phosphate Bioactive Glasses with High Surface Area

MA Peng-Fei[1, 2], LI Ri-Hong[1], ZHANG Long[1]

(1. Key Laboratory of Materials for High Power Laser, Shanghai Institute of Optics and Fine Mechanics, Chinese Academy of Science, Shanghai 201800, China; 2. University of Chinese Academy of Sciences, Beijing 100039, China)

Abstract: High surface area mesoporous bioactive glasses (MBGs) with composition CaO-Al_2O_3-P_2O_5 were fabricated using a simple aqueous Sol-Gel method without any template. Structural characterization of the phosphate-based MBGs was performed by BET, DTA, XRD and FTIR, and MBGs' *in vitro* bioactivity was evaluated by soaking them in simulate body fluid for up to 15 d at 36.5℃. The highest specific surface area is found to be 461.1 m^2/g for the MBG with 5mol% CaO, and it decreased with increasing CaO content. And the glass structure for all the samples was confirmed by XRD and FTIR. However, the MBG with 20mol% CaO exhibits the best *in vitro* bioactivity using simulated body fluid among all samples. The unique combination of a higher specific surface area and relatively high CaO content enables mesoporous calcium aluminum phosphate bioactive glasses to be promising candidates for biomedical applications.

Key words: mesoporous; phosphate glass; bioactive; Sol-Gel

Bioactive glasses are materials which are supposed to achieve the biomedical aim of scaffold preparation[1-3], dental restorations[4-5], drug loading[6-7], coating of metal and polymer implants[8-9], *etc*. Optimal bioactivity, biocompatibility and degradation property are key features for bioactive glasses[10-11]. The method of increasing the specific surface area to improve these features of bioactive glass by Sol-Gel is efficient and remains a favorite among the scientific community[12-13].

Bioactive glasses with a desired pore size, porosity and the pore interconnectivity are needed to serve as a physical support to guide the formation of the new bone tissue. Indeed, the adhesive substrate for implanted cells is supplied *via* the structure of the porous space across the materials[14-16]. The nanoscale pores in the bioactive glass play an important role in promoting cell adhesion, and the adsorption of the biological metabolites and release of useful elements in materials is accelerated due to the porosity[17-18]. Among the porous materials, mesoporous materials with pore size between 2 nm and 50 nm attracts more attentions for using as bioactive glass to repair the defective bone, owing to their high specific surface area, high pore volume and superior bioactive[19-21].

So far, the major reported Sol-Gel-derived mesoporous bioactive glasses have been prepared by surfactant or template depend on the peculiar chelation of metal precursors in aqueous solution for the first, which leads to partial crystallization after the calcination of the gelatin at high temperature[22-23]. Thus upon degradation of the implant, small crystalline particles still exist which can cause sterile inflammation, which has been reported clinically[24-25].

Phosphate-based bioactive glasses have emerged as promising bone substitute materials for bone tissue engineering applications because their chemical composition is very close to that of natural bone, and the rate of dissolution in end application can be more easily modified[26-27]. Moreover, the addition of an appropriate amount of alumina to phosphate-based bioactive glasses can control their dissolution rate and increase mechanical properties and bioactivity[28-30].

The aim here was to develop a phosphate bioactive glass with mesoporous structure in Sol-Gel route. In the present work, mesoporous calcium aluminum phosphate bioactive glasses were synthesized through the Sol-Gel method, free of the annexing agent.

Received date: 2016-03-14; **Modified date:** 2016-06-03
Foundation item: National Natural Science Foundation of China (1308491G00)
Biography: MA Peng-Fei (1989–), male, candidate of Master degree. E-mail: mapf@shanghaitech.edu.cn
Corresponding author: ZHANG Long, professor. E-mail: lzhang@siom.ac.cn
LI Ri-Hong, associate professor. E-mail: lirihong@siom.ac.cn

1 Experimental

1.1 Preparation of MBG

Calcium aluminum phosphate samples were prepared *via* the method of Sol-Gel in aqueous solutions, using aluminum lactate (95%, Sigma), calcium nitrate (99%, Aladdin), and H_3PO_4 (2 mol/L) as precursors. H_3PO_4 (2 mol/L) solution was prepared by dissolving solid H_3PO_4 (99%, Sigma) into ultrapure water. The buffer of hydrochloric acid (1 mol/L, diluted from concentrated hydro-chloric acid, Aladdin) and ammonia solution (1 mol/L,diluted from concentrated ammonia solution, Aladdin) were used to control the value of pH with 0.01 U by a pH meter (Mettler-Toledo pH S20, Switzerland). The nominal molar compositions of the samples are given in Table 1. Gelation was sintered in muffle furnace (Nabertherm, Germany).

1.2 Characterization of MBG

N_2 adsorption/desorption isotherms were obtained at 77.3 K using an automatic surface area analyzer (Quadra-Sorb Station, USA), under continuous adsorption conditions. The *t*-Plot analysis method was used to calculate the pore volume. And the pore size distribution was calculated by the Barretet-Joyner-Halenda (BJH) method. The crystallinity was checked *via* X-ray powder diffraction according to Bragg equation, using Ni-filtered Cu Kαl radiation (λ=0.154 nm). Data were collected in the range 10°< 2θ< 90°, with a time step of 50 s and a step size of 0.02°, at condition of 40 kV and 40 mA. The analysis of Fourier transform infrared spectroscope (FTIR, TENSOR 37, Bruker, German) was carried out using potassium bromide pellets. The pellets were prepared by mixing the sample with potassium bromide (1:100=MBG : KBr, weight ratio). And the spectra were recorded in the range of 1500-400 cm^{-1}. The differential thermal analysis (DTA) was conducted on EXSTAR (S2 6000, Japan), in air at a heating rate of 10 ℃/min up to a maximum temperature of 1000℃.

1.3 *In vitro* bioactive test

The ability of the MBGs to forming the HCA crystals was measured by the *in vitro* bioactivity test. By calculating[19], the glass were ground and 250 mg of the powder samples were soaking in 50 mL simulated body fluid (SBF) solution for series different time intervals (3 d, 7 d, 14 d). After soaking, the solutions were centrifuge at 8000 r/min for 10 min, and the sediments were dried at 100℃ for 8 h in order to be characterized by XRD in the range from 25° to 50°.

2 Results and discussion

2.1 Analysis of the porous structure

As seen from the Fig. 1 and Fig. 2, the N_2 adsorption/desorption isotherms and pore size distribution of the different glasses are obtained. The surface area and the pore size decrease with the increasing content of calcium oxide. Figure 1 shows that all the samples present the type IV adsorption isotherm behavior with a large type H1 hysteresis loop (corresponding to cylindrical), except the glass with 30mol% content of calcium oxide. The sample with 5mol% content of calcium oxide presents the highest specific surface area, reaching 480 m^2/g (Table 2). As the content of calcium oxide increases to 10 mol%, the specific surface area decreases to 280 m^2/g rapidly. However, since the content of the calcium oxide varying from 10mol%–20 mol%, the variance of specific surface area is tiny, just varying from 332.6.6–246.2 m^2/g. As the content of calcium oxide continues to increasing from 20mol% to 25mol%, the specific surface area value decreases rapidly again from 246.2 to 125.7 m^2/g. Indeed, the specific surface area decreases to 25.6 m^2/g, as the content of calcium oxide increases to 30mol%.

As seen from the Fig. 2, the trend of pore size performs the same to the specific surface area in the wake of the increasing content of calcium oxide. As the contents of calcium oxide increases from 5mol% to 10mol%, the pore size varies from 50 nm to 32 nm rapidly. However, the variance of pore size is small with the content of calcium oxide continuous increasing to 20mol%. With the content of calcium oxide continuous increasing to 30mol%, the pore size changes rapidly. Porous structure becomes extreme scarcity, when the content of calcium oxide increases to 30mol%.

Table 1 The phosphate coding, corresponding molar composition, annealing temperature and T_c temperature

Glass code	CaO/mol%	$AlO_{3/2}$/mol%	$PO_{5/2}$/mol%	Annealing, *T*/℃	T_c(℃) (glass), *T*/℃
5%CaO-MBG	5	45	50	600	806.75
10%CaO-MBG	10	40	50	600	738.00
15%CaO-MBG	15	35	50	600	728.08
20%CaO-MBG	20	30	50	600	717.66
25%CaO-MBG	25	25	50	600	709.58
30%CaO-MBG	30	20	50	600	701.10

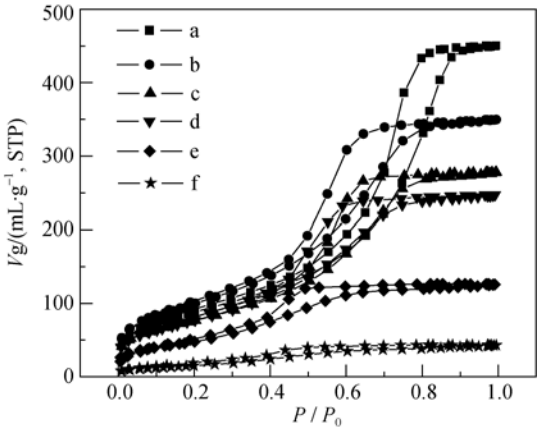

Fig. 1 N_2 adsorption/desorption isotherms with different content samples
a) 5%CaO-MBG; b) 10%CaO-MBG; c) 15%CaO-MBG; d) 20%CaO-MBG; e) 25%CaO-MBG; f) 30%CaO-MBG

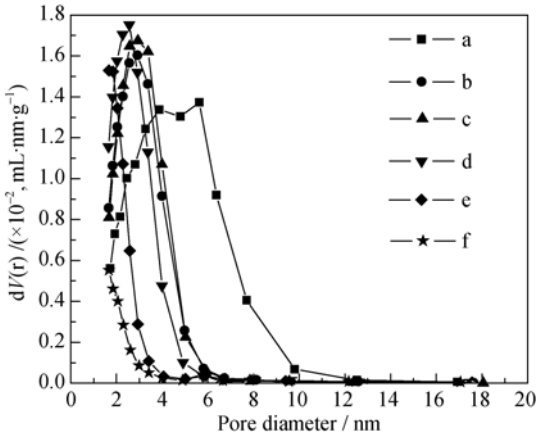

Fig. 2 The pore size distribution of different samples
a) 5%CaO-MBG; b) 10%CaO-MBG; c) 15%CaO-MBG; d) 20%CaO-MBG; e) 25%CaO-MBG; f) 30%CaO-MBG

Table 2 Specific surface area, pore volume and pore size of the series sample of different samples

Glass code	Specific surface area/ ($m^2 \cdot g^{-1}$)	Pore volume/ ($mL \cdot g^{-1}$)	Pore size/nm
5%CaO-MBG	461.1	0.697	4.3
10%CaO-MBG	332.6	0.412	3.0
15%CaO-MBG	251.3	0.421	2.9
20%CaO-MBG	246.2	0.380	2.7
25%CaO-MBG	125.7	0.195	2.3
30%CaO-MBG	25.6	0.066	1.9

2.2 The analysis of DTA

Fig. 3 shows the DTA traces collected for the different compositions with the increasing calcium oxide. And the T_c temperatures are presented in Table 1. Due to the Sol-Gel methods and the thermal treatment at 600℃, the T_g temperature can't be reflected clearly from the tracts of DTA. As seen from the Fig. 3, a decrease in T_c temperature is obtained with increasing content of calcium oxide.

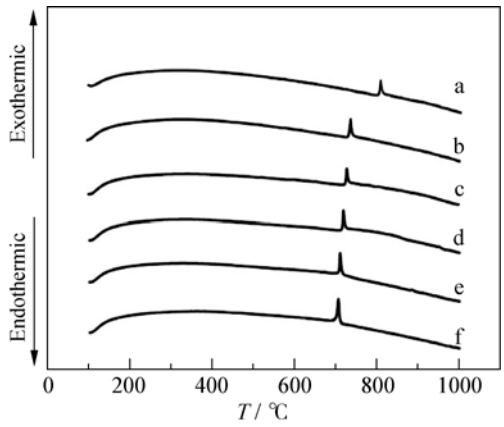

Fig. 3 The DTA curves of different samples
a) 5%CaO-MBG; b) 10%CaO-MBG; c) 15%CaO-MBG; d) 20%CaO-MBG; e) 25%CaO-MBG; f 30%CaO-MBG

Notably, all the T_c temperature of the different glasses is above 600℃. And the lowest T_c temperature is about 701.1℃ for the sample of the highest calcium oxide content (30mol%). Therefore, the samples can remain the structure of glass at the heat treatment temperature of 600℃, avoiding crystallization.

2.3 Analysis of the XRD patterns

Typical X-Ray Diffraction patterns of the phosphate glasses are given in Fig. 4. Apparently, sharp diffraction peak don't appear in the patterns of mesoporous materials. The sole broad diffraction peak at ~20°–30° (2θ value) in the all patterns, illuminating the main constituent of the mesoporous materials is amorphous phosphate structure[12]. After the low temperature treatment, MBGs always consist of amorphous phase, regardless of the increasing amount of calcium oxide in samples.

2.4 Analysis of the FTIR spectra

Fig. 5 shows the FTIR spectra of the phosphate glass samples. Almost no change is seen in the samples with the increasing content of calcium oxide. Each FTIR spectra shows the characteristic 490 cm^{-1} which correspond to the

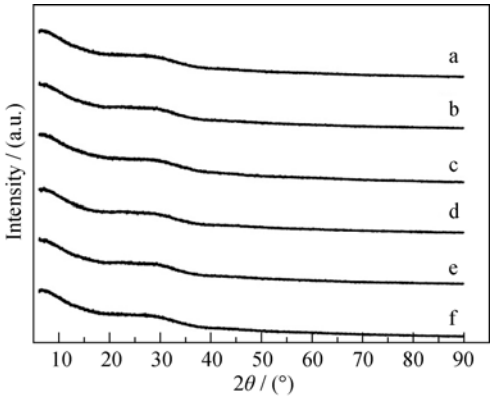

Fig. 4 XRD natterns of samples
a) 5%CaO-MBG; b) 10%CaO-MBG; c) 15%CaO-MBG; d) 20%CaO-MBG; e) 25%CaO-MBG; f) 30%CaO-MBG

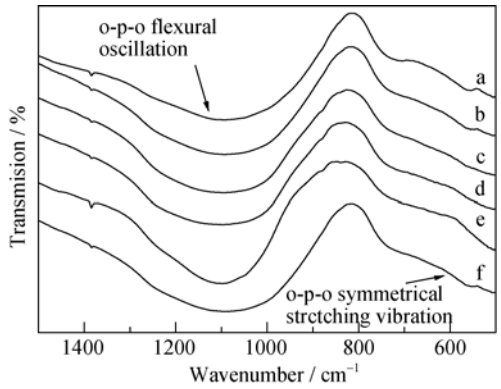

Fig. 5 FTIR spectra of different samples

a) 5%CaO-MBG; b) 10%CaO-MBG; c) 15%CaO-MBG; d) 20%CaO-MBG; e) 25%CaO-MBG; f) 30%CaO-MBG

flexural vibration of the O–P–O bond correspond to P=O at 1250 cm^{-1}, which appears on the occasion of crystallization in phosphate glass, proving the amorphous form of phosphate glass. The result of FTIR spectra is in line with the conclusion of X-Ray diffraction patterns.

2.5 Analysis of bioactive *in vitro* study

Fig. 6 shows the XRD patterns of the samples with the increasing content of calcium oxide before and after soaking in SBF solution. The presence of a broad band between 20° and 30° (2θ value) with no diffraction is observed, which confirms the amorphous structure of the phosphate matrix of glasses without dipping in SBF. After soaking, the major hydroxyapatite diffraction peaks

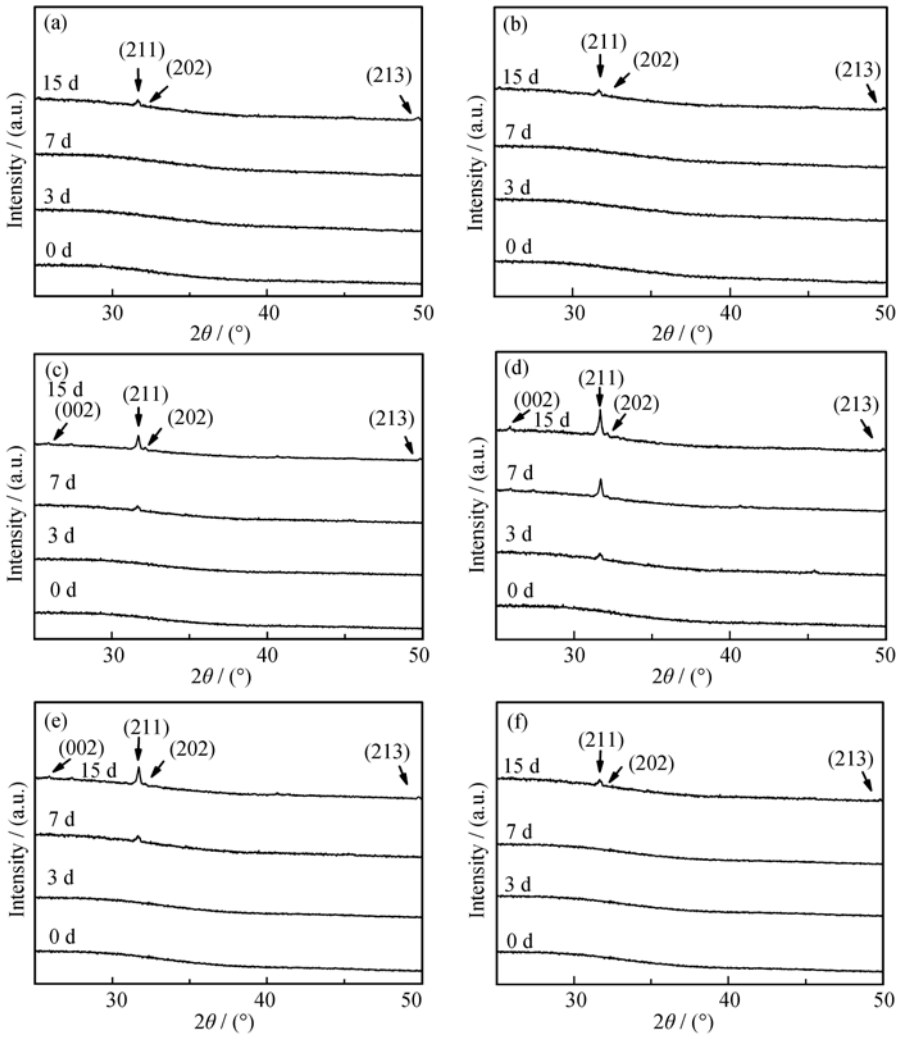

Fig. 6 XRD patterns of the samples before and after soaking in SBF solution

a) 5%CaO-MBG; b) 10%CaO-MBG; c) 15%CaO-MBG; d) 20%CaO-MBG; e) 25%CaO-MBG; f) 30%CaO-MBG

[JCPDS 09-0432] (International Center for Diffraction Data, Swarthmore, PA, 2002) on the patterns at the different time periods, illustrating the change bioactive of the varying content glasses.

According to the XRD patterns of the series time in the SBF, the appearing time of hydroxyapatite diffraction peaks becomes early with the increasing calcium oxide content from 5mol% to 20mol%. The results suggest that more content of calcium, which is one of the major elements in bone tissue, can improve the bioactive the mesoporous calcium aluminum phosphate glasses. However, as the content of calcium increases from 20mol% to 30mol%,

30mol%, the speed of forming the hydroxyapatite becomes slow. In consideration of the tendency of porous properties with increasing the content of calcium oxide, lower specific surface area maybe the significant factor to reduce the bio active of phosphate glass

After 3 d soaking, a clear diffraction peak at 32° (2θ value), which could be assigned to the (211) HCA reflection, was first revealed in the MBG with the 20mol% content of calcium oxide. As the soaking time goes on, several marked diffraction peaks appeared which could be recognized as the (022), (310) and (213) HCA reflections. Under the influence of between the mesoporous characteristic and the content of calcium, the glasses with 20mol% content of calcium oxide performed the best bioactive.

3 Conclusions

1) MBGs CaO-Al_2O_3-P_2O_5 were fabricated in Sol-Gel route, with the advantage of the unique characteristic of high specific surface areas and the absence of any surfactant or template depend on the peculiar chelation of metal precursors in aqueous solution for the first. Due to their advantages over their solid-state counterparts, porous materials can be designed and used to carrier drugs. Because of their high specific surface area and large pore volume, high drug loading and controlling over the rate and period of delivery are their main advantages. Their bioactivity can be improved significantly by tailoring bioactive inorganic materials into a porous structure.

2) With the increasing calcium oxide, the T_c temperature and specific surface area decreases. However, the major phase is amorphous structure for all samples, and the mesoporous structure still exist with CaO content increasing to 25mol%.

3) The results of the SBF experiments suggested that the mesoporous calcium aluminum phosphate glass containing 20mol% calcium oxide perform the best bioactivity, due to higher specific surface area and its more calcium oxide. The result can be used as guidance to design the expected structure in order to obtain the optimal ability for biotechnological application.

References:

[1] QUINLAN E, PARTAP S, AZEVEDO M M, *et al*. Hypoxia-mimicking bioactive glass/collagen glycosaminoglycan composite scaffolds to enhance angiogenesis and bone repair. *Biomaterials*, 2015, **52:** 358–366.

[2] LIU HUI, CHEN XIAO-FENG, LI XIAN, *et al*. Gene transfection of bioactive glass fibers. *Journal of Inorganic Materials*, 2014, **29(10):** 1023–1028.

[3] ZHU Y, SHANG F, LI B, *et al*. Magnetic mesoporous bioactive glass scaffolds: preparation, physicochemistry and biological properties. *Journal of Materials Chemistry B*, 2013, **1(9):** 1279–1288.

[4] ZHI-HONG D, ZHI-PING N, CHANG-CHUN Z. Bionic remineralization of acidic etched enamel induced by using mesoporous bioactive glass in natural oral saliva. *Journal of Inorganic Materials*, 2016, **31(1):** 88–94.

[5] AJITA J, SARAVANAN S, SELVAMURUGAN N. Effect of size of bioactive glass nanoparticles on mesenchymal stem cell proliferation for dental and orthopedic applications. *Materials Science and Engineering: C*, 2015, **53:** 142–149.

[6] LI Y, LIU Y Z, LONG T, *et al*. Mesoporous bioactive glass as a drug delivery system: fabrication, bactericidal properties and biocompatibility. *Journal of Materials Science: Materials in Medicine*, 2013, **24(8):** 1951–1961.

[7] HUANG S, KANG X, CHENG Z, *et al*. Electrospinning preparation and drug delivery properties of Eu^{3+}/Tb^{3+} doped mesoporous bioactive glass nanofibers. *Journal of Colloid and Interface Science*, 2012, **387(1):** 285–291.

[8] WANG X, WEN C. Corrosion protection of mesoporous bioactive glass coating on biodegradable magnesium. *Applied Surface Science*, 2014, **303:** 196–204.

[9] AL-NOAMAN A, RAWLINSON S C F, HILL R G. The role of MgO on thermal properties, structure and bioactivity of bioactive glass coating for dental implants. *Journal of Non-Crystalline Solids*, 2012, **358(22):** 3019–3027.

[10] JONES J R. Review of bioactive glass: from Hench to hybrids. *Acta Biomaterialia*, 2013, **9(1):** 4457–4486.

[11] YANG G J, LIN M, ZHANG L, *et al*. Progress of calcium sulfate and inorganic composites for bone defect repair. *Journal of Inorganic Materials*, 2013, **28(8):** 795–803.

[12] SHRUTI S, SALINAS A J, MALAVASI G, *et al*. Structural and in vitro study of cerium, gallium and zinc containing Sol–Gel bioactive glasses. *Journal of Materials Chemistry*, 2012, **22(27):** 13698–13706.

[13] CHEN J, QUE W, XING Y, *et al*. Molecular level-based bioactive glass-poly (caprolactone) hybrids monoliths with porous structure for bone tissue repair. *Ceramics International*, 2015, **41(2):** 3330–3334.

[14] HENDRIKX S, KASCHOLKE C, FLATH T, *et al*. Indirect rapid prototyping of sol-gel hybrid glass scaffolds for bone regeneration-effects of organic crosslinker valence, content and molecular weight on mechanical properties. *Acta Biomaterialia*, 2016, **35:**

318–329.

[15] TAI H, MATHER M L, HOWARD D, *et al*. Control of pore size and structure of tissue engineering scaffolds produced by supercritical fluid processing. *Eur. Cell Mater.*, 2007, **14:** 64–77.

[16] OKII N, NISHIMURA S, KURISU K, *et al*. *In vivo* histological changes occurring in hydroxyapatite cranial reconstruction. *Neurologia Medico-Chirurgica*, 2001, **41(2):** 100–104.

[17] EMADI R, TAVANGARIAN F, ESFAHANI S I R, *et al*. Nanostructured forsterite coating strengthens porous hydroxyapatite for bone tissue engineering. *Journal of the American Ceramic Society*, 2010, **93(9):** 2679–2683.

[18] FATHI M H, DOOSTMOHAMMADI A. Bioactive glass nanopowder and bioglass coating for biocompatibility improvement of metallic implant. *Journal of Materials Processing Technology*, 2009, **209(3):** 1385–1391.

[19] HENCH L L. Sol-Gel materials for bioceramic applications. *Current Opinion in Solid State and Materials Science*, 1997, **2(5):** 604–610.

[20] WANG X, LI X, ITO A, *et al*. Synthesis and characterization of hierarchically macroporous and mesoporous CaO-MO-SiO_2-P_2O_5 (M= Mg, Zn, Sr) bioactive glass scaffolds. *Acta Biomaterialia*, 2011, **7(10):** 3638–3644.

[21] MA Z, DONG G, LV C, *et al*. Core-shell glass fibers with high bioactivity and good flexibility. *Materials Letters*, 2012, **88:** 136–139.

[22] POOLOGASUNDARAMPILLAI G, WANG D, LI S, *et al*. Cotton-wool-like bioactive glasses for bone regeneration. *Acta Biomaterialia*, 2014, **10(8):** 3733–3746.

[23] CUI Y, LI H, YI K, *et al*. Moisture absorption characteristics of a SiO_2 film from 2 to 3 μm. *Chinese Optics Letters*, 2015, **13(2):** 023101.

[24] KNOWLES J C, FRANKS K, ABRAHAMS I. Investigation of the solubility and ion release in the glass system K_2O-Na_2O-CaO-P_2O_5. *Biomaterials*, 2001, **22(23):** 3091–3096.

[25] KOKUBO T, TAKADAMA H. How useful is SBF in predicting *in vivo* bone bioactivity. *Biomaterials*, 2006, **27(15):** 2907–2915.

[26] AHMED I, LEWIS M, OLSEN I, *et al*. Phosphate glasses for tissue engineering: part 2. Processing and characterisation of a ternary-based P_2O_5–CaO–Na_2O glass fibre system. *Biomaterials*, 2004, **25(3):** 501–507.

[27] FRANKS K, ABRAHAMS I, GEORGIOU G, *et al*. Investigation of thermal parameters and crytallisation in a ternary CaO-Na_2O-P_2O_5-based glass system. *Biomaterials*, 2001, **22(5):** 497–501.

[28] SMITH J M, KING S P, BARNEY E R, *et al*. Structural study of Al_2O_3-Na_2O-CaO-P_2O_5 bioactive glasses as a function of aluminium content. *The Journal of Chemical Physics*, 2013, **138(3):** 034501.

[29] EL-KHESHEN A A, KHALIAFA F A, SAAD E A, *et al*. Effect of Al_2O_3 addition on bioactivity, thermal and mechanical properties of some bioactive glasses. *Ceramics International*, 2008, **34(7):** 1667–1673.

[30] THIND K S, SINGH K, SHARMA G, *et al*. Influence of addition of Al_2O_3 on physical, structural, acoustical and *in-vitro* bioactive properties of phosphate glasses. *Physica Status Solidi (a)*, 2009, **206(7):** 1447–1455.

溶胶–凝胶法制备高比表面积铝磷钙生物活性玻璃

马鹏飞[1,2], 李日红[1], 张 龙[1]

(1. 中国科学院 上海光学精密机械研究所, 强激光材料重点实验室, 上海 201800; 2. 中国科学院大学, 北京 100049)

摘 要: 采用溶胶–凝胶法, 在不使用模板剂的情况下制备出高比表面积的介孔 CaO-Al_2O_3-P_2O_5 生物活性玻璃(MBGs), 用 BET、XRD、DTA 以及 FTIR 对 MBGs 的结构进行了表征, 并用生物模拟体液(SBF)在 36.5℃对生物玻璃进行了体外活性测试, 测试时间为 1 d、3 d、7 d 和 14 d。介孔玻璃的比表面积最高达到 461.1 m^2/g, 随着 CaO 的含量从 5mol%增加到 30mol%, 介孔玻璃的比表面积呈降低趋势。用 XRD 和 FTIR 验证了材料的玻璃结构。然而, 在生物模拟体液(SBF)实验中, 当 CaO 摩尔含量达到 20mol%时, 介孔玻璃表现出较高生物活性。这种特殊的高比表面积的介孔铝磷钙生物活性玻璃在生物医药方面有潜在的应用价值。本文的实验结果对优化生物玻璃的介孔结构和 CaO 含量来提升玻璃的生物活性有一定的指导意义。

关 键 词: 介孔结构; 磷酸盐玻璃; 生物活性; 溶胶–凝胶

中图分类号: TQ174 **文献标识码:** A